

The Reductive Leaching of Chalcopyrite by Chromium(II) Chloride for the Rapid and Complete Extraction of Copper

Jonathan T. Vardner,^{*,[a]} Yuta Inaba,^[a] Heejung Jung,^[a] Raymond S. Farinato,^[b] D. R. Nagaraj,^[b] Scott Banta,^[a] and Alan C. West^[a, b]

A hydrometallurgical process is developed to lower the costs of copper production and thereby sustain the use of copper throughout the global transition to renewable energy technologies. The unique feature of the hydrometallurgical process is the reductive treatment of chalcopyrite, which is in contrast to the oxidative treatment more commonly pursued in the literature. Chalcopyrite reduction by chromium(II) ion is described for the first time and superior kinetics are shown. At high concentrate loadings of 39, 78, and 117 gL⁻¹, chalcopyrite

reacted completely within minutes at room temperature and pressure. The XRD, SEM-EDS, and XPS measurements indicate that chalcopyrite reacts to form copper(I) chloride (CuCl). After the reductive treatment, the mineral products are leached by iron(III) sulfate to demonstrate the complete extraction of copper. The chromium(II) ion may be regenerated by an electrolysis unit inspired by an iron chromium flow battery in a practical industrial process.

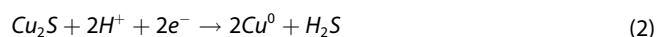
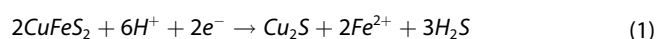
Introduction

The increasing demand for copper coincides with declining grades of copper reserves, and consequently, a global peak in copper production is expected to arise in the coming decades.^[1] Alternative processing routes for chalcopyrite (CuFeS₂), which accounts for approximately 70% of the world's copper reserves, may extend the availability of copper throughout the 21st century. The pyrometallurgical process is generally used in industry to convert CuFeS₂ to metallic Cu despite relatively high investment and operating costs.^[2] The smelting step is generally considered to be environmentally deleterious due to the release of sulfur dioxide, carbon dioxide as well as the potential release of arsenic and other toxic elements. Industry and academia have sought to replace the pyrometallurgical process with a hydrometallurgical alternative for economic and environmental sustainability.^[2]

Hydrometallurgical processes include bioleaching,^[3-10] high temperature and pressure leaching,^[11,12] the Galvanox process^[13-16] and many other variants thereof, the majority of them using ferric ion and sulfuric acid. The kinetics of CuFeS₂ bioleaching, and leaching in general, from ores or concentrates in a sulfate (or sulfuric acid) medium are hindered by a passivating sulfur-like or metal-deficient layer; consequently,

leaching efficiency is poor. High temperature pressure leaching overcomes the passivation, but such conditions are often uneconomical in many plants. The galvanox process is a promising alternative to enhance copper recovery at atmospheric pressure and relatively low temperature but has not seen widespread adoption by industry. It should be noted that there are other processes in various phases of development that may become promising alternatives.^[17,18]

The electrolytic conversion of CuFeS₂ to copper may be a more promising route for its hydrometallurgical processing.^[19] CuFeS₂ can be electrochemically reduced to less refractory mineral phases for copper extraction.^[20-24] Equations (1) and (2) show that CuFeS₂ can be electrochemically reduced to Cu₂S and, subsequently, to Cu. These reactions have undergone a number of optimizations by modifying the electrolyte, separator, electrode materials, and reactor design.^[25]




Reactions 1 and 2 [Eqs. (1) and (2)] are in direct competition with the hydrogen evolution reaction, and therefore typically operate at Faradaic efficiencies below 40%. These slurry reactions also present potential engineering challenges such as reactor plugging and electrode fouling.^[25]

The chemical reduction of CuFeS₂ may be advantageous because it obviates the hydrogen evolution reaction and circumvents engineering challenges associated with slurry electrodes. The chemical reduction of CuFeS₂ has been tested with Fe,^[26] Cu,^[27] Al,^[28] and SO₂^[29] as reductants. These reducing agents generally require high temperatures or small particle sizes, and therefore, have not been adopted by industry. In this work, Cr²⁺ was tested as a reductant for the first time and superior kinetics are demonstrated. Although the cost of chromium is high relative to copper, an electrolysis unit inspired

[a] Dr. J. T. Vardner, Dr. Y. Inaba, Dr. H. Jung, Prof. S. Banta, Prof. A. C. West
Department of Chemical Engineering
Columbia University
New York, NY 10027 (USA)
E-mail: jtv2115@columbia.edu

[b] Prof. R. S. Farinato, Prof. D. R. Nagaraj, Prof. A. C. West
Department of Earth and Environmental Engineering
Columbia University
New York, NY 10027 (USA)

 © 2023 The Authors. Published by Wiley-VCH GmbH. This is an open access article under the terms of the Creative Commons Attribution License, which permits use, distribution and reproduction in any medium, provided the original work is properly cited.

by an iron chromium flow battery (ICFB)^[30–35] may be leveraged to efficiently regenerate the Cr^{2+} at high current densities.

Results and Discussion

A violent reaction was observed upon adding the CuFeS_2 concentrate to the solution of 1 M CrCl_2 and 4 M HCl . Reaction 3 [Eqs. (3)] is postulated to be taking place and is discussed throughout this section.



Figure 1 shows the pictures of the reaction between 1 M CrCl_2 , 4 M HCl , and 78 g L⁻¹ CuFeS_2 concentrate after 0, 2, 3, 5, and 60 s of reaction time. The pictures show the rapid release

of H_2S gas, which was qualitatively measured with a *Sensorcon* detector. The release of gas ensued immediately upon the addition of the concentrate and concluded within a minute of reaction time. The liquid phase samples were measured with gas chromatography–mass spectroscopy (GC-MS) to confirm the presence of dissolved H_2S for similar experiments.

The evolution of gaseous H_2S coincided with the release of Fe^{2+} ions to solution, which is consistent with Reaction 3 [Eqs. (3)]. Figure 2a shows the percent of Fe^{2+} released as a function of time for a slurry comprising 1 M CrCl_2 , 4 M HCl , and CuFeS_2 concentrate loadings of 39, 78, 117, and 234 g L⁻¹. The reaction kinetics were rapid considering that approximately 100% of Fe^{2+} was released from CuFeS_2 within 5 min for the CuFeS_2 concentrate loadings of 39, 78 and 117 g L⁻¹. The release of Fe^{2+} , however, was limited for the CuFeS_2 concentrate loading of 234 g L⁻¹ suggesting the complete utilization of Cr^{2+} .

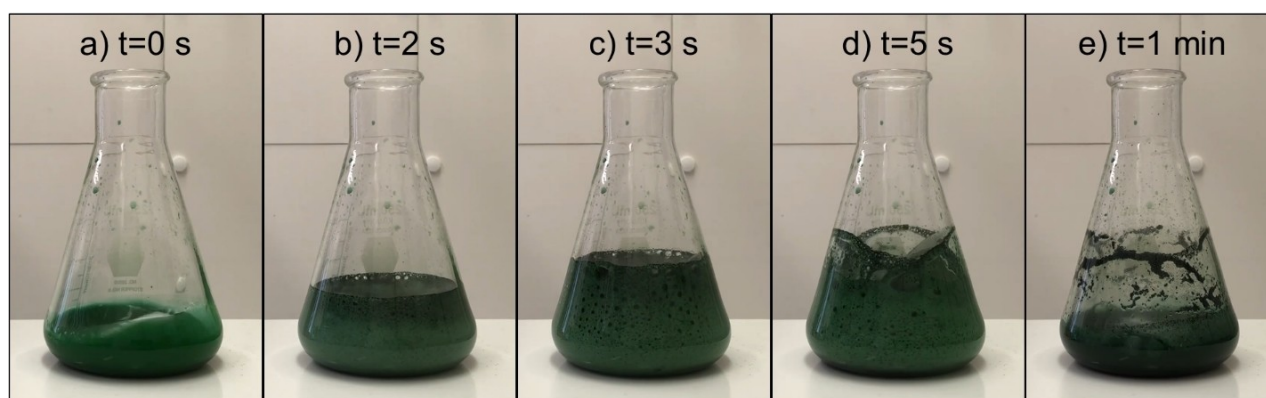


Figure 1. Pictures of the reaction between 1 M CrCl_2 , 4 M HCl and 78 g L⁻¹ of the CuFeS_2 concentrate at a) 0 s, b) 2 s, c) 3 s, d) 5 s, and e) 1 min.

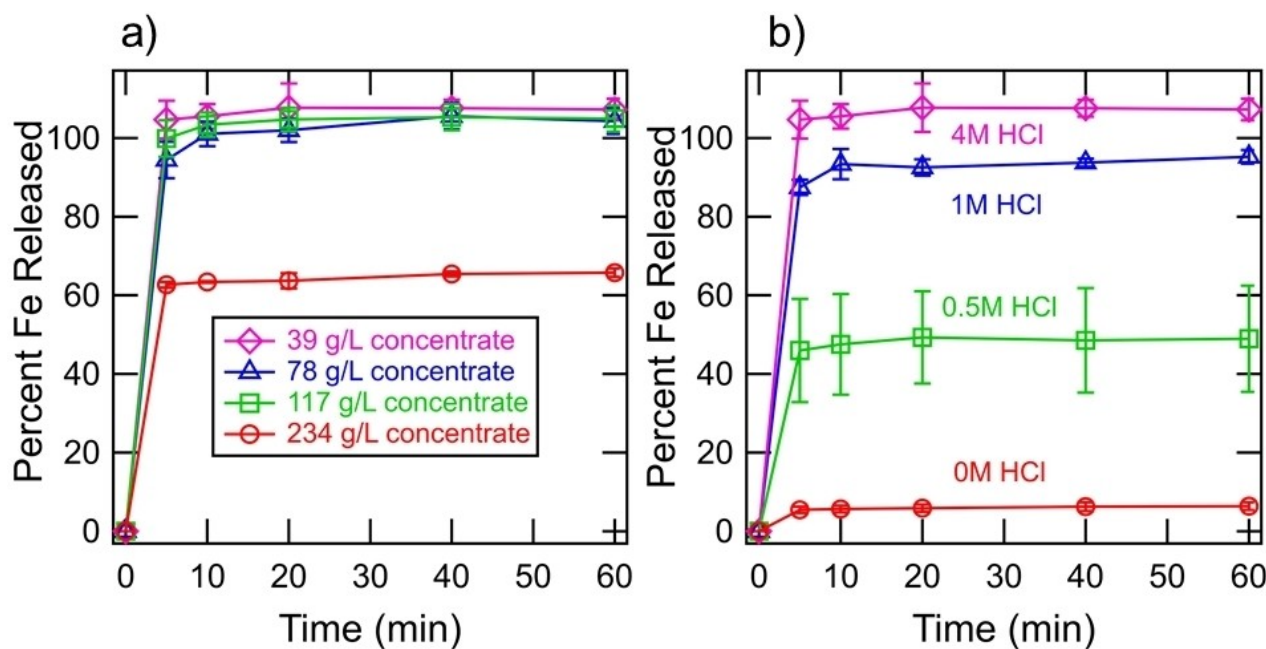


Figure 2. (a) Release of Fe^{2+} ions to solution during the progression of the reaction between 1 M CrCl_2 , 4 M HCl , and various loadings of CuFeS_2 concentrate. (b) Release of Fe^{2+} ions to solution during the progression of the reaction between 1 M CrCl_2 , 39 g L⁻¹ CuFeS_2 concentrate, and various initial concentrations of HCl . Error bars show the standard deviations of replicates in triplicate.

Measurements of Fe^{2+} release exceeding 100% may indicate a minor error in the estimation of composition shown in Table 1, due to both the error in XRD quantification and the sieving of the concentrate to be within 53–106 μm . The experiments were conducted while purging the headspace of the reactor with argon and similar results were observed, indicating that small amount of oxygen present in the system did not oxidize Cr^{2+} to any significant level. The release of copper ions to solution during the progression of the reaction was measured, but the quantitative results were inconsistent due to the precipitation of the ions out of solution, which is discussed below. The copper ions are thought to be released in the form of Cu^+ , rather than Cu^{2+} , due to the reductive conditions of the electrolyte and presence of the chloride ion for stability. The pH of the solutions after the reduction experiments were below zero, ensuring that these reactions were not pH limited. The Cu^{2+} ion is not thought to be present due to the reductive conditions in the electrolyte.

Figure 2b shows the percent of Fe^{2+} released as a function of time for slurries comprising 1 M CrCl_2 , 39 g L^{-1} of CuFeS_2 concentrate, and initial HCl concentrations of 0 M, 0.5 M, 1 M, and 4 M. The pH of the solution after the reduction step was approximately 2.5 for the slurries with initial HCl concentrations of 0 M, 0.5 M, 1 M, indicating that these reactions were pH limited. The pH of the solution after the reduction step may be leveraged to facilitate a separation between Fe^{2+} and Cr^{3+} , which may be desirable prior to the reduction of Cr^{3+} to Cr^{2+} by an electrolysis unit. These results suggest that the proton has a greater stoichiometric number than CuFeS_2 , which is consistent with Reaction 3 [Eqs. (3)]. The experiments conducted with initial HCl concentrations of 2 M and 3 M were found not to be pH limited.

Figure 3 shows images of the mineral products after 60 min of reduction with the Cr^{2+} ion obtained with a Keyence VHX-5000 microscope. The results indicate that the mineral product is affected by the CuFeS_2 concentrate loading. The 39 g L^{-1} CuFeS_2 loading yielded a green product, which is consistent with the appearance of CuCl as well as other potential Cu–Cl complexes. The various mineral products were characterized and shown to yield different amounts of copper recovery, which is discussed below. The mineral products post reaction with various HCl concentrations yielded the same trend in appearance.

Figure 4 shows the XRD spectra for the various chalcopyrite concentrate loadings subsequent to reaction with the Cr^{2+} ion, and Figure 5 shows the XRD spectra for the mineral samples subsequent to reaction with the Cr^{2+} ion and various initial HCl

Table 1. Mineralogy of concentrate supplied by Freeport-McMoRan.		
Mineral	Chemical Formula	Percent
Chalcopyrite	CuFeS_2	78.3
Pyrite	FeS_2	12.9
K-feldspar	KAlSi_3O_8	2.9
Plagioclase	$\text{NaAlSi}_3\text{O}_8$	2.9
Quartz	SiO_2	2.2
Molybdenite	MoS_2	0.85

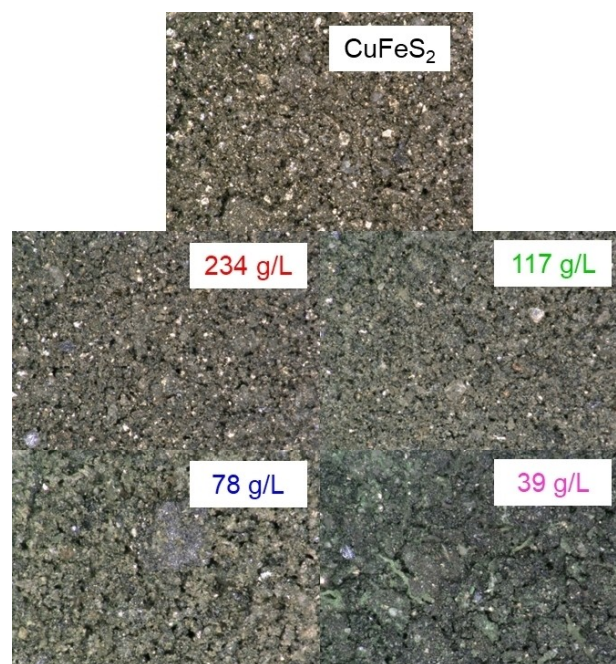


Figure 3. Optical microscopy images of the mineral products after reaction between various chalcopyrite concentrate loadings, 1 M CrCl_2 and 4 M HCl for 60 min.

concentrations. The predominant peaks of the unreacted CuFeS_2 concentrate were consistent with CuFeS_2 , FeS_2 , and SiO_2 , as shown in Table 1. The relative intensity of the peaks associated with CuFeS_2 diminished for the reacted mineral products, consistent with the Fe^{2+} release measured by AAS. The peaks associated with the reaction products emerged for the mineral products with high conversion of CuFeS_2 . The predominant mineral product was determined to be copper chloride (CuCl) from the spectra. Secondary products, such as $\text{Cu}_2(\text{OH})_3\text{Cl}$, were consistent with the spectra. Reaction 4 [Eqs. (4)] shows the precipitation of CuCl out of solution, which is the primary product formed. Reaction 4 is shown for simplicity whereas the chemistry taking place is more complicated and a variety of Cu–Cl complexes precipitate. The precipitation of CuCl out of the solution containing 4 M HCl was unexpected considering that the molar ratio of Cl/Cu was 36 in the system. However, the molar ratio of Cl/Cr was 6, and therefore, complexes formed between Cl^- and Cr^{3+} may lower the number of Cl^- ions available to stabilize Cu^+ . The concentration of Cu^+ in solution after 60 min of reduction was approximately 0.07 M, which is close to the solubility limit of 0.233 M reported at 2 M HCl in the literature.^[36] It is estimated that 40% of copper in the system remained in the bulk solution as Cu^+ and 60% precipitated out of solution for the experiments conducted with a concentrate loading of 39 g L^{-1} and an acid concentration of 4 M HCl.



The XRD data, in conjunction with the AAS data, indicate that the FeS_2 and silicates were inert during the reductive

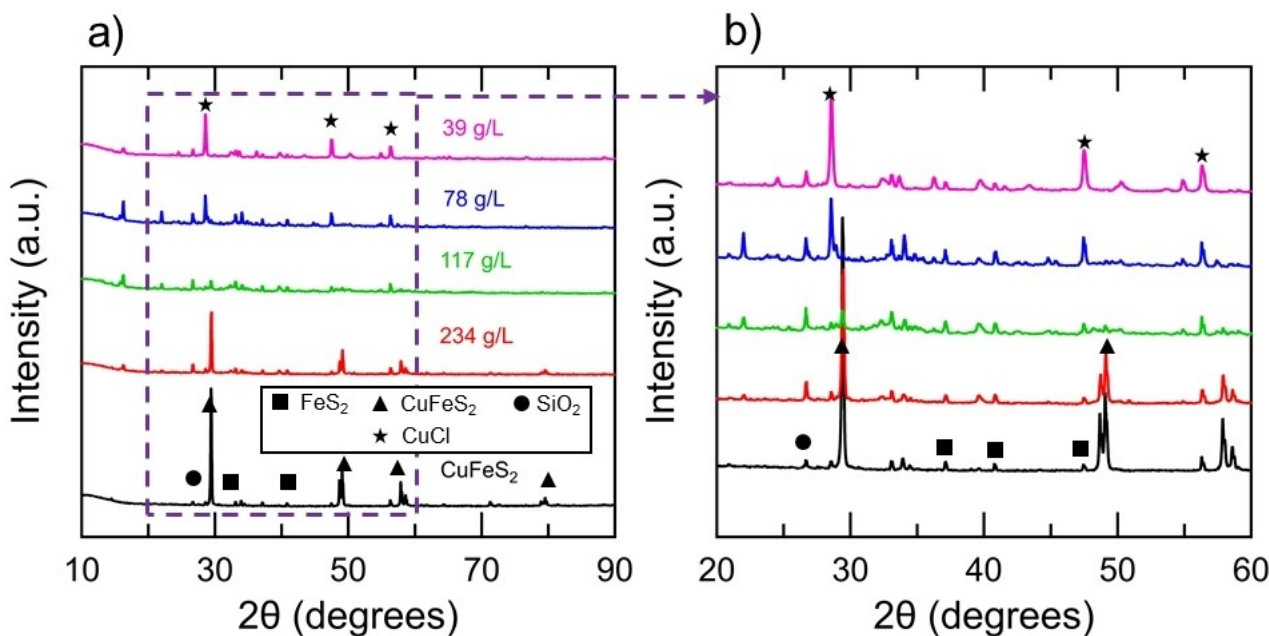


Figure 4. XRD results for the mineral products after reaction between various chalcopyrite concentrate loadings, 1 M CrCl₂ and 4 M HCl for 60 min. (b) Close-up of region used to identify mineral products.

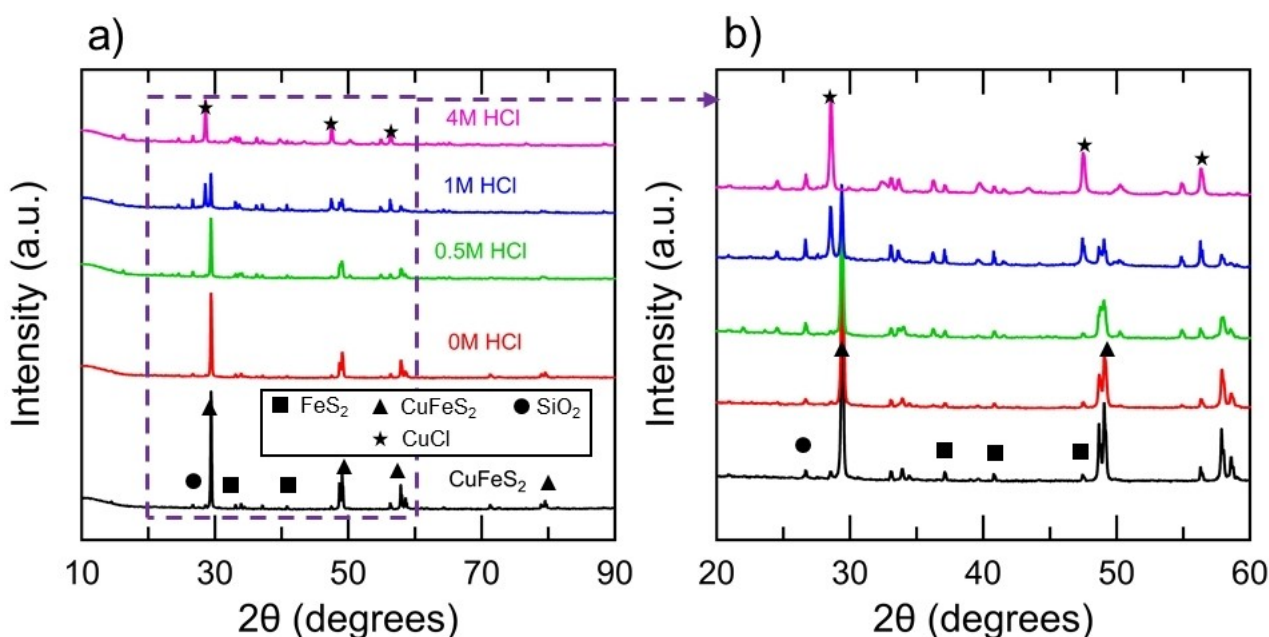


Figure 5. (a) XRD results for the mineral products after reaction between 39 g L⁻¹ of the chalcopyrite concentrate with 1 M CrCl₂ and various initial concentrations of HCl for 60 min. (b) Close-up of region used to identify mineral products.

treatment. Experiments were conducted between 39 g L⁻¹ CuFeS₂ concentrate, 1 M CrCl₂, 4 M HCl and initial ferrous chloride (FeCl₂) concentrations of 0, 0.5 M, 1 M, and 2 M. It was determined that the reduction process can tolerate initial FeCl₂ concentrations of 1 M and below. The Fe²⁺ precipitated out of solution for the experiment conducted with an initial FeCl₂ concentration of 2 M.

Figure 6 shows SEM results for the mineral products after reaction with 1 M CrCl₂ and 4 M HCl for 60 min. The mineral

products develop some mossy features, which may be related to the growth of CuCl. Figure 7 shows EDS results for the mineral samples post reduction with the Cr²⁺ ion. The unreacted CuFeS₂ concentrate samples show peaks corresponding to Cu, Fe, S, Si, and O. The reacted samples show the diminishment in the Fe and S peaks, which is consistent with the release of Fe²⁺ to solution and the release of H₂S as a gas. The minor S peak present in the 39 g L⁻¹ sample may be related to the presence of unreacted FeS₂ in the mineral products. The

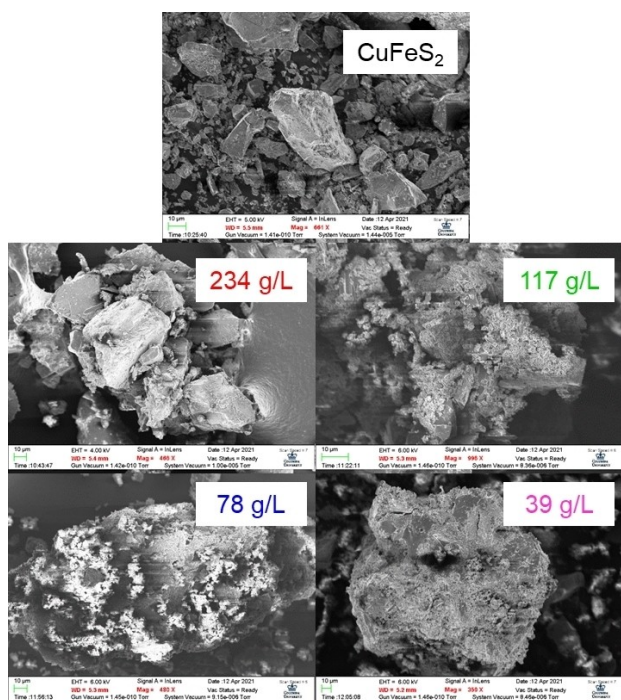


Figure 6. SEM images of mineral products after reaction with 1 M CrCl₂ and 4 M HCl for 60 min.

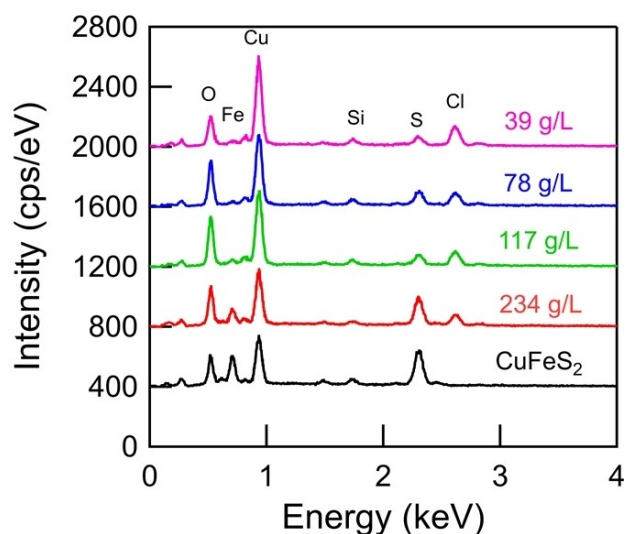
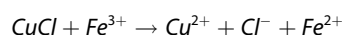


Figure 7. EDS results for the mineral products after reaction with 1 M CrCl₂ and 4 M HCl for 60 min.

reacted samples also show the emergence of the Cl peak, which is consistent with the formation of CuCl. The Cu peak elongates for the reacted samples due to the increasing mass fraction of Cu within the samples. No peak corresponding to Cr was observed in the spectra, indicating that the presence of Cr within the samples is minor. The samples were digested in aqua regia and the mass fraction of Cr within the samples was estimated to be 1–3%. The presence of chromium is thought to be an artifact of the procedure used to filter and dry the mineral products.

Figure 8 shows the XPS spectra of Cu and Cl for the mineral samples post reduction with the Cr²⁺ ion. The Cr element was not observed on the mineral products, which further indicates that the samples were not comprised of chromium. Similarly, Fe and S were not observed on the surface of the mineral reaction products, which is consistent with the release of Fe²⁺ and H₂S from the surface of the particles into the solution phase. The XPS data indicate the absence of a sulfur passivation layer, which may account for the rapid kinetics of the reduction reaction. The various copper peaks indicate the presence of several copper-containing products leading to convoluted spectra. For instance, the peaks at the binding energies of 944 and 935 eV are assigned to Cu₂(OH)₃Cl and CuCl, respectively. The Cu scans also show an observable shift in binding energy from the CuFeS₂ concentrate standard. The emergence of a Cl peak for the reacted samples is consistent with the formation of Cu–Cl complexes.

Figure 9 shows the extraction of Cu²⁺ from the mineral products by 0.5 M Fe₂(SO₄)₃. Reaction 5 [Eqs. (5)] shows the leaching reaction of CuCl by the Fe³⁺ oxidant, which goes to completion within minutes.



The results show that virtually all of the Cu²⁺ can be extracted from the 39 g L⁻¹ mineral product. The aqueous solution may subsequently undergo solvent extraction and electrowinning for the production of metallic copper. In experiments, not shown, the 39 g L⁻¹ sample was solubilized to the same extent in 1 M H₂SO₄, and therefore, the ferric ion may not be required for the extraction of copper. The incomplete copper extraction for higher pulp densities is partly related to the incomplete conversion of CuFeS₂ shown in Figure 2. Also, potential intermediates formed, such as Cu₂(OH)₃Cl, may be refractory for copper leaching and undesirable. It is shown that virtually no Cu²⁺ is extracted from the CuFeS₂ concentrate, and therefore, the reductive treatment directly leads to the extraction of copper.

Conclusions

Chalcopyrite concentrate was reduced by CrCl₂ in acid solution for the first time and superior kinetics were shown at room temperature and ambient pressure. AAS was used to measure the complete release of Fe²⁺ from CuFeS₂ within minutes during its reduction. XRD and SEM-EDS were used to characterize the predominant mineral product to be CuCl. The measurements also indicate that pyrite and silicates were inert during the reductive treatment. XPS was used to measure the surface of the mineral products and the results suggest that the rapid kinetics may be related to the lack of a passivation layer during the reduction step. The mineral products were leached by the ferric ion to demonstrate complete copper recovery.

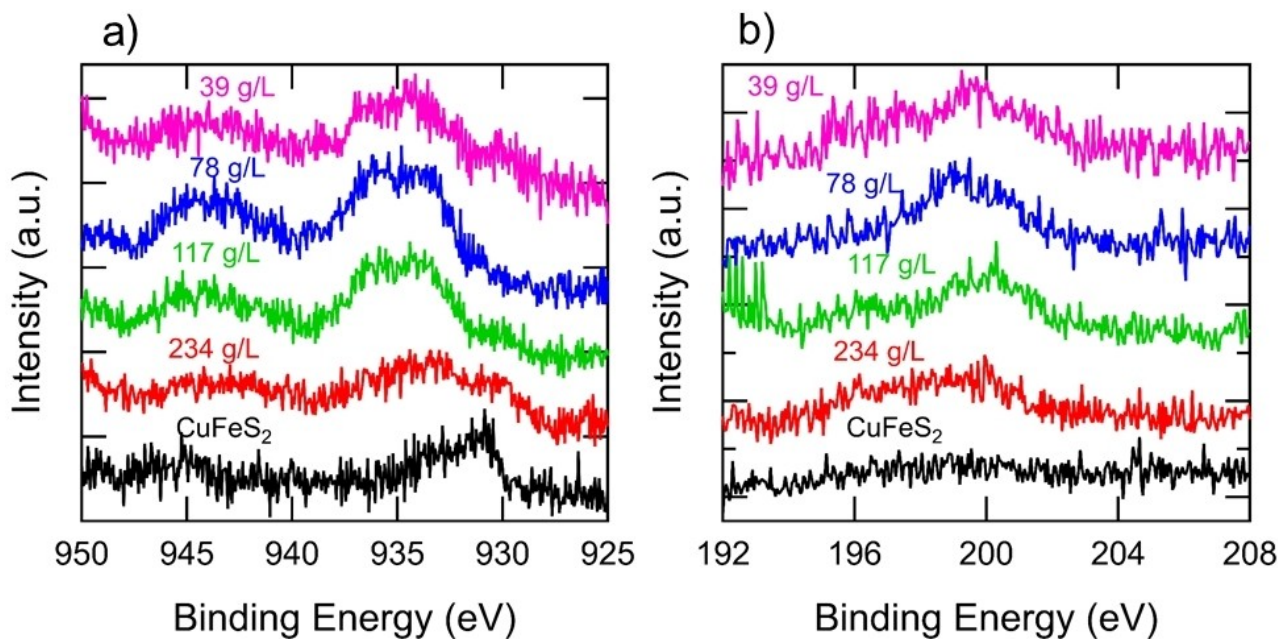


Figure 8. XPS results for mineral products after reaction with 1 M CrCl_2 and 4 M HCl for 60 min for (a) Cu and (b) Cl.

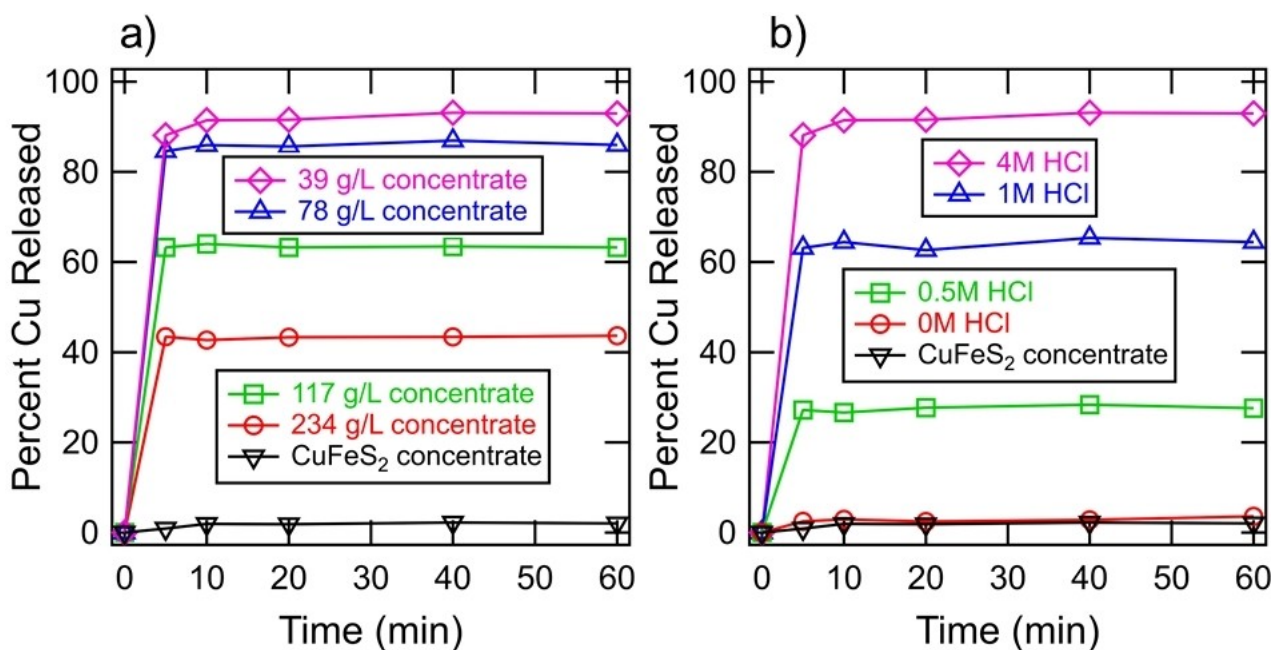


Figure 9. (a) Extraction of Cu^{2+} from mineral products by 0.5 M $\text{Fe}_2(\text{SO}_4)_3$ subsequent to the reaction between 1 M CrCl_2 , 4 M HCl, and various loadings of CuFeS_2 concentrate. (b) Extraction of Cu^{2+} from mineral products by 0.5 M $\text{Fe}_2(\text{SO}_4)_3$ subsequent to reaction between 1 M CrCl_2 , 39 g L^{-1} CuFeS_2 concentrate, and various initial concentrations of HCl.

Experimental Section

Reduction of CuFeS_2

Chalcopyrite mineral concentrate was kindly provided by *Freeport-McMoRan*. It was analyzed by the supplier with energy dispersion X-ray diffraction to have the following composition as shown in Table 1.

The CuFeS_2 concentrate was sieved ($-140+270$ mesh) to confine the particle size to be within 53–106 μm . An amount of 50 g of the concentrate was subsequently rinsed with 1 L of DI water and 1 L of 1 M H_2SO_4 to remove any soluble iron and copper ions generated during natural concentrate oxidation occurring in transport and storage. CuFeS_2 concentrate pulp densities of 39, 78, 117, or 234 g L^{-1} were added to a 250 mL Erlenmeyer flask containing 25 mL of a solution comprising of 1 M CrCl_2 and 4 M HCl. For other experiments, a CuFeS_2 concentrate pulp density of 39 g L^{-1} was added to a solution comprising 1 M CrCl_2 and various HCl

concentrations. Thirdly, for other experiments, a CuFeS_2 concentrate pulp density of 39 g L^{-1} was added to a solution comprising of 1 M CrCl_2 , 4 M HCl , and various concentrations of FeCl_2 . It was imperative for the reaction to be conducted in a fume hood due to the rapid release of H_2S gas, as shown in Figure 1. Liquid phase $100 \mu\text{L}$ samples were taken at time points of 0, 5, 10, 20, 40, and 60 min, which were subsequently diluted for the measurements of Fe^{2+} and Cu^+ contents. After the reduction, the mineral particles were filtered from solution and allowed to air dry prior to characterization.

Atomic Absorption Spectroscopy (AAS)

An *ICE 3300* AAS was used to measure the release of Fe^{2+} and Cu^+ ions into solution from CuFeS_2 during its reduction. The characteristic wavelengths for the iron and copper measurements were 248.3 nm and 324.8 nm , respectively. Standards ranging from 0–4 ppm were measured immediately before the samples to construct linear ($R^2 > 0.995$) calibration curves.

X-ray Diffraction (XRD)

A PANalytical XPert3 Powder XRD was used to measure the bulk mineral phase of the reaction products. The XRD was operated with filtered Empyrean $\text{Cu K}\alpha$ radiation ($k=0.15418 \text{ nm}$), a tube voltage of 45 kV , and a current of 40 mA . The mineral products were placed on a silicon crystal zero-diffraction plate (MTI Corporation) and were adhered in place with Apiezon grease. The samples were scanned continuously in the range of $10\text{--}100^\circ$ with a step size of 0.0065° on a spinning plate with a revolution time of 2.0 s . A PIXcel1D detector was used to record the peak intensity for the subsequent analysis of the mineral composition.

X-ray Photoelectron Spectroscopy (XPS)

A *PHI 5500* XPS equipped with an Al X-ray source was used to measure the elemental composition of the reaction product surfaces. The base pressure of the chamber was approximately 1×10^{-8} torr. Samples were supported on carbon tape.

Scanning Electron Microscopy – Energy Dispersion X-ray Spectroscopy (SEM-EDS)

A *Zeiss Sigma VP* SEM was used to capture images of the mineral products after reaction. The SEM-EDS analysis was operated at an accelerating potential of 6 kV and base pressure of approximately 1×10^{-5} torr. Samples were supported on carbon tape and were coated with gold using a *Cressington 108 Auto Sputter Coater*. The sputtering was conducted under argon gas flow with 0.1 mbar of pressure for 20 s . A *Bruker XFlash Detector* was used for EDS analysis to analyze elemental composition.

Subsequent Leaching of Mineral Products

A sample of the mineral products was digested in aqua regia for complete copper extraction, and an equivalent sample of the mineral products was leached in a solution comprising $0.5 \text{ M Fe}_2(\text{SO}_4)_3$ in $1 \text{ M H}_2\text{SO}_4$. The percent of copper released was determined by the ratio of copper extracted by the two leachants.

Acknowledgements

This material is based upon work supported by the National Science Foundation Graduate Research Fellowship under grant No. (DGE – 1644869). Any opinion, findings, and conclusions or recommendations expressed in this material are those of the authors and do not necessarily reflect the views of the National Science Foundation. This work was also supported by ARPA-E grant DE-AR0001340 from the US Department of Energy. The authors gratefully acknowledge Freeport-McMoRan for providing the chalcopyrite mineral concentrate.

Conflict of Interest

The authors declare no conflict of interest.

Data Availability Statement

Research data are not shared.

Keywords: chalcopyrite · copper · electrochemistry · hydrometallurgy · leaching

- [1] R. A. Kerr, *Science* **2014**, *343*, 722–724.
- [2] M. E. Schlesinger, M. J. King, K. C. Sole, W. G. Davenport, *Extractive Metallurgy of Copper*, 5th edition, Elsevier, Oxford **2011**.
- [3] G. Gu, K. Hu, X. Zhang, X. Xiong, H. Yang, *Electrochim. Acta* **2013**, *103*, 50–57.
- [4] M. Khoshkhoo, M. Dopson, A. Shchukarev, Å. Sandström, *Hydrometallurgy* **2014**, *149*, 220–227.
- [5] H. Liu, J. Xia, Z. Nie, *Hydrometallurgy* **2015**, *156*, 40–46.
- [6] H. Yuehua, Q. Guanzhou, W. Jun, W. Dianzuo, *Hydrometallurgy* **2002**, *64*, 81–88.
- [7] L. Zhang, J. Wu, Y. Wang, L. Wan, F. Mao, W. Zhang, X. Chen, H. Zhou, *Hydrometallurgy* **2014**, *146*, 15–23.
- [8] H. Zhao, Y. Zhang, X. Zhang, L. Qian, M. Sun, Y. Yang, Y. Zhang, J. Wang, H. Kim, G. Qiu, *Miner. Eng.* **2019**, *136*, 140–154.
- [9] H.-B. Zhou, W.-M. Zeng, Z.-F. Yang, Y.-J. Xie, G.-Z. Qiu, *Bioresour. Technol.* **2009**, *100*, 515–520.
- [10] W. Zhu, J. Xia, Y. Yang, Z. Nie, L. Zheng, C. Ma, R. Zhang, A. Peng, L. Tang, G. Qiu, *Bioresour. Technol.* **2011**, *102*, 3877–3882.
- [11] R. G. McDonald, D. M. Muir, *Hydrometallurgy* **2007**, *86*, 206–220.
- [12] R. G. McDonald, D. M. Muir, *Hydrometallurgy* **2007**, *86*, 191–205.
- [13] G. Nazari, D. G. Dixon, D. B. Dreisinger, *Hydrometallurgy* **2011**, *105*, 251–258.
- [14] G. Nazari, D. G. Dixon, D. B. Dreisinger, *Hydrometallurgy* **2012**, *111–112*, 35–45.
- [15] G. Nazari, D. G. Dixon, D. B. Dreisinger, *Hydrometallurgy* **2012**, *113–114*, 122–130.
- [16] G. Nazari, D. G. Dixon, D. B. Dreisinger, *Hydrometallurgy* **2012**, *113–114*, 177–184.
- [17] X. Ge, X. Wang, S. Seetharaman, *Electrochim. Acta* **2009**, *54*, 4397–4402.
- [18] G. Granata, A. Miura, W. Liu, F. Pagnanelli, C. Tokoro, *Hydrometallurgy* **2019**, *186*, 244–251.
- [19] K. Daehn, A. Allanore, *Curr. Opin. Electrochem.* **2020**, *22*, 110–119.
- [20] T. Biegler, D. C. Constable, *J. Appl. Electrochem.* **1977**, *7*, 175–179.
- [21] T. Biegler, D. A. Swift, *J. Appl. Electrochem.* **1976**, *6*, 229–235.
- [22] J. C. Fuentes-Aceituno, G. T. Lapidus, F. M. Doyle, *Hydrometallurgy* **2008**, *92*, 26–33.
- [23] V. J. Martínez-Gómez, J. C. Fuentes-Aceituno, R. Pérez-Garibay, J. Lee, *Hydrometallurgy* **2016**, *164*, 54–63.
- [24] V. J. Martínez-Gómez, J. C. Fuentes-Aceituno, R. Pérez-Garibay, J. Lee, *Hydrometallurgy* **2018**, *181*, 195–205.

- [25] C. A. Donnelly, J. T. Vardner, Z. Zhang, S. Banta, A. C. West, *JOM* **2020**, 72, 3818–3825.
- [26] D. Dreisinger, N. Abed, *Hydrometallurgy* **2002**, 66, 37–57.
- [27] J. B. Hiskey, M. E. Wadsworth, *Metall. Mater. Trans. B* **1975**, 6, 183–190.
- [28] F. Doyle, G. Lapidus, *ECS Trans.* **2006**, 2, 189.
- [29] H.-J. Sohn, M. E. Wadsworth, *JOM* **1980**, 32, 18–22.
- [30] Y. K. Zeng, T. S. Zhao, L. An, X. L. Zhou, L. Wei, *J. Power Sources* **2015**, 300, 438–443.
- [31] Y. K. Zeng, X. L. Zhou, L. An, L. Wei, T. S. Zhao, *J. Power Sources* **2016**, 324, 738–744.
- [32] S. Wang, Z. Xu, X. Wu, H. Zhao, J. Zhao, J. Liu, C. Yan, X. Fan, *Appl. Energy* **2020**, 271, 115252.
- [33] C.-Y. Sun, H. Zhang, *Int. J. Energy Res.* **2019**, 43, 8739–8752.
- [34] Y. K. Zeng, X. L. Zhou, L. Zeng, X. H. Yan, T. S. Zhao, *J. Power Sources* **2016**, 327, 258–264.
- [35] Y. K. Zeng, T. S. Zhao, X. L. Zhou, L. Zeng, L. Wei, *Appl. Energy* **2016**, 182, 204–209.
- [36] J. J. Fritz, *J. Chem. Eng. Data* **1982**, 27, 188–193.

Manuscript received: September 6, 2022
Revised manuscript received: November 30, 2022